REPORT DOCUMENTATION PAGE

Form Approved
OMB No. 0704-0188

1. REPORT DATE *(DD-MM-YYYY)*	**2. REPORT TYPE**	**3. DATES COVERED** *(From - To)*
June 2013	Technical Paper	June 2013-July 2013

4. TITLE AND SUBTITLE
Kinetics Modeling of Hypergolic Propellants

5a. CONTRACT NUMBER

5b. GRANT NUMBER

5c. PROGRAM ELEMENT NUMBER

6. AUTHOR(S)
Sardeshmukh, S., Heister, S., Wang, H. and Sankaran, V.

5d. PROJECT NUMBER

5e. TASK NUMBER

5f. WORK UNIT NUMBER
Q12M

7. PERFORMING ORGANIZATION NAME(S) AND ADDRESS(ES)

Air Force Research Laboratory (AFMC)
AFRL/RQR
5 Pollux Drive
Edwards AFB CA 93524-7048

8. PERFORMING ORGANIZATION REPORT NO.

9. SPONSORING / MONITORING AGENCY NAME(S) AND ADDRESS(ES)
Air Force Research Laboratory (AFMC)
AFRL/RQR
5 Pollux Drive
Edwards AFB CA 93524-7048

10. SPONSOR/MONITOR'S ACRONYM(S)

11. SPONSOR/MONITOR'S REPORT NUMBER(S)
AFRL-RQ-ED-TP-2013-173

12. DISTRIBUTION / AVAILABILITY STATEMENT
Distribution A: Approved for Public Release; Distribution Unlimited. PA#13436

13. SUPPLEMENTARY NOTES
Conference paper for the 49th AIAA/ASME/SAE/ASEE Joint Propulsion Conference, San Jose, CA, 15-17 July 2013.

14. ABSTRACT

Multi-phase ignition of hypergolic propellants Mono-methyl Hydrazine (MMH) and Red Fuming Nitric Acid (RFNA) is studied numerically to understand fundamental processes such as gas phase ignition, vaporization and liquid phase chemistry for characterizing ignition. Such understanding will be critical for future design efforts targeting rapidly repeatable cyclic ignition of these propellants. Three test cases are considered: gas and liquid phase autoignition, an opposed jet diffusion flame and a liquid opposed jet diffusion flame. For the first case, three reduced chemical kinetics mechanisms are used to study autoignition behavior in the gas phase and with premixed liquids. In the second case, a laminar diffusion flame of the gas phase reactants under varying strain rates is studied. The third case investigates the interface behavior for liquid-liquid contact and its effect on gas phase ignition.

15. SUBJECT TERMS

16. SECURITY CLASSIFICATION OF:			**17. LIMITATION OF ABSTRACT**	**18. NUMBER OF PAGES**	**19a. NAME OF RESPONSIBLE PERSON**
					Venkateswaran Sankaran
a. REPORT	**b. ABSTRACT**	**c. THIS PAGE**	SAR	19	**19b. TELEPHONE NO** *(include area code)*
Unclassified	**Unclassified**	**Unclassified**			661-525-5534

Standard Form 298 (Rev. 8-98)
Prescribed by ANSI Std. 239.18

Kinetics Modeling of Hypergolic Propellants

Swanand V. Sardeshmukh,* Stephen D. Heister,† Haifeng Wang,‡
and Venkateswaran Sankaran,§

Multi-phase ignition of hypergolic propellants Mono-methyl Hydrazine (MMH) and Red Fuming Nitric Acid (RFNA) is studied numerically to understand fundamental processes such as gas phase ignition, vaporization and liquid phase chemistry for characterizing ignition. Such understanding will be critical for future design efforts targeting rapidly repeatable cyclic ignition of these propellants. Three test cases are considered: gas and liquid phase autoignition, an opposed jet diffusion flame and a liquid opposed jet diffusion flame. For the first case, three reduced chemical kinetics mechanisms are used to study autoignition behavior in the gas phase and with premixed liquids. In the second case, a laminar diffusion flame of the gas phase reactants under varying strain rates is studied. The third case investigates the interface behavior for liquid-liquid contact and its effect on gas phase ignition.

Nomenclature

MMH	Mono-Methyl Hydrazine (CH_3NHNH_2)
$RFNA$	Red Fuming Nitric Acid (88%HNO_3, 10%N_2O_4 and 2%H_2O)
O/F	Oxidizer to Fuel ratio by weight
t	Time, s
μ	Molecular viscosity, $Pa\,s$
χ	Mole fraction
Y	Mass fraction
λ	Thermal conductivity, $W/\,m\,K$
MW	Molar mass, $kg/\,kmol$
D	Molecular diffusivity, $m^2/\,s$
ρ	Density, $kg/\,m^3$
p	Pressure, Pa
T	Temperature, K
h	Enthalpy, $J/\,kg$
s	Entropy, $J/\,kg\,K$
$\dot{\omega}$	Production (destruction) rate of a species, $kmol/\,s$
RANS	Reynolds Averaged Navier-Stokes equations
DES	Detached Eddy Simulation
LES	Large Eddy Simulation
GEMS	General Equation and Mesh Solver
Subscript	
j	Species number
k	Reaction number

*Doctoral student, School of Mechanical Engineering, 701 W. Stadium Ave. W. Lafayette, IN-47907, student member, AIAA.

†Raisbeck Engineering Distinguished Professor, School of Aeronautics and Astronautics, Director, Maurice J. Zucrow Laboratories, 701 W. Stadium Ave. West Lafayette, IN 47907, Fellow, AIAA.

‡Assistant Professor, School of Aeronautics and Astronautics, 701 W. Stadium Ave. West Lafayette, IN 47907, member AIAA.

§Senior Scientist, Rocket Propulsion Division, Air Force Research Laboratory (AFRL), Room 203-C, Bldg 8351, 4 Draco Drive Edwards AFB, CA 93524, USA, Senior Member, AIAA.

I. Introduction

The ignition behavior of hypergolic propellants is of importance for rocket applications that require multiple restarts and/or thrust control. Additionally the high specific impulse and low energy requirement for storage at atmospheric conditions make these propellants a prime candidate for small, maneuverable rocket applications. One such set of propellants is monomethyl hydrazine (MMH) and red fuming nitric acid (RFNA) which are liquids at atmospheric conditions. The ignition delay of these propellants is an important parameter and its analytical understanding is desirable for developing new designs as well as advanced control strategies. Such understanding requires multi-physics modeling which in turn depends upon the knowledge of the sub-phenomena involved in the ignition process. The goal of present work is to characterize the underlying physics and to develop a modeling methodology for investigating hypergolic ignition of MMH and RFNA.

Early experiments with the hydrazine family of propellants provided system level, empirical understanding of macroscopic effects [1–5]. Saad et al. [6] separated the processes involved as shown in Figure 1 and studied some of the sub-phenomena independently. They reported that the competing processes of liquid vaporization, reaction and the effect of pressure on each are important for hypergolic ignition. Recent studies [7–9] confirm that the hypergolic ignition of MMH and RFNA involves complex sub-phenomena: spray formation upstream of the impingement point, instabilities in the sheets resulting in intermittent liquid contact and aerosol formation, gas layer development between the two liquid sheets due to liquid reaction and vaporization as well as satellite drop interactions and micro-explosions in the outer extremities of the liquid sheets. The rate and extent of each sub-phenomena determine the ultimate outcome for practical systems, in terms of one discernible quantity, namely the ignition delay [10]. Figure 2 shows a schematic representation of some of these sub-phenomena.

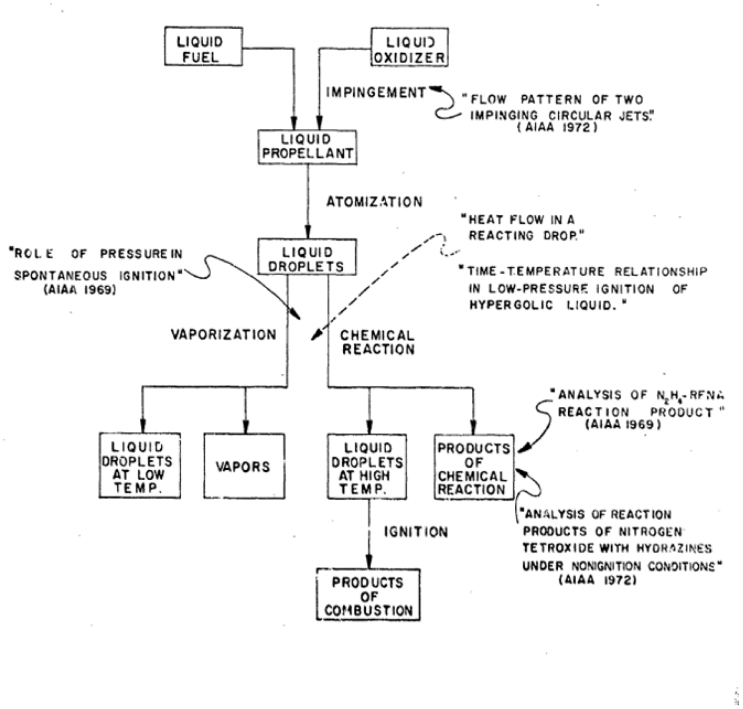

Figure 1: Various processes as described and studied by Saad et. al. [6]

Historically, the hypergolicity of this family of propellants was attributed to thermal activation [11] and the resulting gas intermediates were noted to be important [12]. High speed measurements obtained recently [7] confirm that the gas intermediates are at a temperature of $550\,K$. The compression within the generated gas layer was thought to influence the ignition [13] and the associated delay. Formation and decomposition of solid intermediates was also reported [14–16] and were attributed to be the cause of pressure spikes during re-ignition. The gas phase, known to contribute a large share of the total heat released,

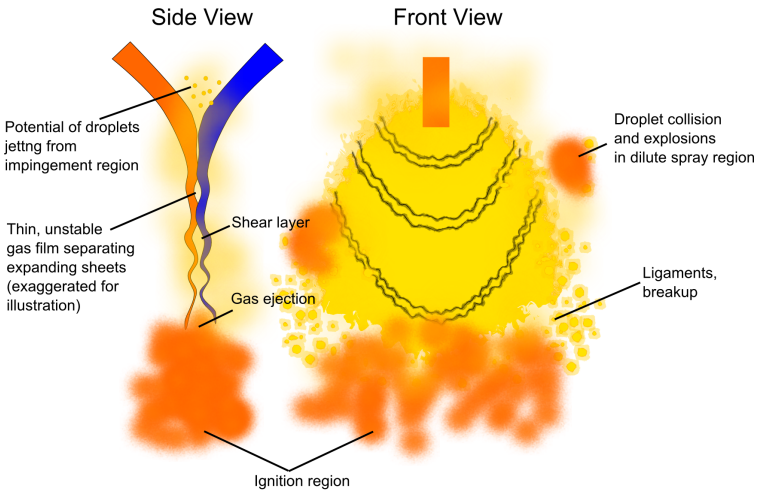

Figure 2: Sub-phenomena involved in the ignition of impinging jets of MMH and RFNA

showed multiple flame regions [11, 17] and was addressed by various experiments [18–20] to develop reaction mechanisms [21, 22]. Recent studies have improved our knowledge of the thermodynamic properties, reaction rates [23–27] and reaction pathways that are of relevance to the hypergolic ignition. However, experimental evidence points to the gas phase ignition being contingent upon the liquid interactions [7, 10, 28] and hence the overall effect must be considered for the accurate prediction of ignition delay.

The time and length scales of the sub-phenomena involved can pose a significant challenge for experimental measurements [9, 29] and high-fidelity physics-based simulations can significantly benefit the understanding. However the use of full chemical kinetics mechanisms in addition to the fluid dynamics can incur significant computational costs due to the large number of species and due to the stiffness introduced by the time scale differences in the chemical reactions. A tangible reduction in this expense can be achieved by reduced chemical mechanisms. Three such mechanisms for MMH-RFNA, due to Labbe et. al. [30, 31] are a recent advance and need to be studied.

As such, hypergolic ignition phenomenon has been an object of study for more than four decades and many of its aspects have been investigated experimentally. However detailed understanding of hypergolic ignition, which is a cumulative effect, is limited due to relatively less efforts on the modeling front. In order to remedy this and use substantial advances in computational methodology, there is a need to establish a modeling framework for hypergolic systems. Following in the footsteps of experimental investigations, gas phase kinetics should be the first, followed by gas-liquid interactions. The overall objective of the paper is thus, to investigate isolated sub-phenomena as well as their coupled impact on the ignition delay while providing a characterization of the three reduced mechanisms.

The present article starts with a brief summary of the CFD solver and the chemical mechanisms used in this study. We then consider a suite of test problems, each of which focuses on a specific aspect of the full model. The test problems include (1) autoignition to study the gas-phase chemical kinetics and the combined effect including reacting, vaporizing liquids; (2) an opposed jet diffusion flame for understanding the kinetics and transport in a diffusion flame, and finally (3) an opposed liquid jet case targeting the impingement region and intervening gas layer. Results and discussion of each part are summarized at the end providing a direction for future efforts.

II. Model

The solver GEMS (General Equations and Mesh Solver with multiple approaches), used in the present work, is a finite volume, time accurate solver capable of handling a generalized fluid(caloric and state equations). A hybrid LES-RANS (Large Eddy Simulation and Reynolds Averaged Navier-Stokes equations) approach is used for turbulence modeling with Wilcox's $k-\omega$ model for the RANS regions and a DES (Detached Eddy Simulation) approach in the resolved regions of the flow. It has an approximate Reimann solver with comprehensive preconditioning and employs the line Gauss Seidel algorithm for the solution of the linear system. A multi-block unstructured mesh is handled in a parallel fashion for two as well as three dimensional solutions. For modeling the liquid phase, the homogeneous equilibrium model, based on Amagat's law is used, whereby the total volume of a fluid is equal to the sum of partial volumes of its components. The liquid phase is then included as a fluid species with a density equal to the liquid phase density. This approach has been successfully demonstrated in previous work for modeling of cavitating flows [32]. The reader is referred to prior articles for further details of the solver [32–36].

A. Equations of Motion

The equations of motion can be written as:

$$\frac{\partial Q}{\partial t}+\frac{\partial E_i}{\partial x_i}-\frac{\partial F_{vi}}{\partial x_i}=H+\Omega \tag{1}$$

where the vector Q is a set of conserved variables, E_i and F_{vi} are the inviscid and viscous flux vectors respectively and the vector H contains the source terms other than in the species equations. The last vector, Ω, contains the sources(or sinks) for the species and is calculated using a kinetics mechanism where the reaction rates are given by the frequently used Arrhenius expression [37],

$$K_f=AT^b e^{\frac{-E_a}{RT}} \tag{2}$$

where k_f is the forward rate of reaction, A, b are constants, T is temperature, E_a is activation energy and R is the universal gas constant. Accurate reaction rate determination can require additional details such as third body efficiencies and low pressure limit rates [38,39]. At low pressures, two sets of Arrhenius parameters are typically specified where the rate k_0 is effective at low pressures and k_∞ at high pressures. For the transition to the high pressure limit ("fall-off" region), the reaction rate can be obtained by,

$$k=k_\infty\left(\frac{P_r}{1+P_r}\right)F \tag{3}$$

where P_r is the reduced pressure scale, given by

$$\frac{k_0\left[M\right]}{k_\infty} \tag{4}$$

and F is the broadening factor, obtained either from the Troe parameters [38] or the Tsang and Herron [40] linear fit. In Troe form, F is given as,

$$\log F=\left[1+\left[\frac{\log\left(P_r\right)+c}{n-d\left(\log P_r+c\right)}\right]^2\right]^{-1}\log\left(F_{cent}\right) \tag{5}$$

where F_{cent} is,

$$F_{cent}=\left(1-\alpha\right)e^{(-T/t_1)}+\alpha e^{(-T/t_2)}+e^{(-t_3/T)} \tag{6}$$

and $\alpha, t_1,\ t_2$ and t_3 are Troe parameters. Other constants in the calculation of F_{cent} are,

$$\begin{aligned} c&=-0.4-0.67\log\left(F_{cent}\right),\\ n&=0.75-1.27\log\left(F_{cent}\right)\\ d&=0.14. \end{aligned} \tag{7}$$

For the Tsang and Herron fit, F is,

$$F = tsa_1 + tsa_2 \times T \tag{8}$$

where tsa_1 and tsa_2 are rate parameters. Once the forward rate is determined, the reverse reaction rate can be obtained from equilibrium constant K_{eq}.

Thermal and transport properties for each species are calculated using the curve-fit tabulations due to McBride et al. [41] with the exception of the molecular diffusivity, which is calculated using Chapman-Enskog theory [42]. Mixture thermal properties are calculated as mass weighted averages while the mixture transport properties are found using mixing rules due to Hirschfelder and Wilke, modified by Bird [43, 44] and Mathur [45]. According to these modifications, the molecular diffusivity, D_{j-mix}, of any species j into the mixture is given as,

$$D_{j-mix} = \frac{1 - Y_j}{\sum_{l,l\neq j}^{N} X_l / D_{lj}}. \tag{9}$$

Mixture viscosity is calculated using the relation:

$$\mu = \sum_{j=1}^{N} \frac{X_j \mu_j}{\sum_{l=1}^{N} X_l \phi_{jl}} \tag{10}$$

where the function ϕ is defined as,

$$\phi_{jl} = \frac{1}{\sqrt{8}} \left(1 + \left(\frac{\mu_j}{\mu_l}\right)^{1/2} \left(\frac{MW_l}{MW_j}\right)^{1/4}\right)^2 \left(1 + \frac{MW_j}{MW_l}\right)^{-1/2}. \tag{11}$$

The thermal conductivity of the mixture is,

$$\lambda = \frac{1}{2} \left(\sum_{j=1}^{N} X_j \lambda_j + \frac{1}{\sum_{l=1}^{N} \frac{X_l}{\lambda_l}} \right) \tag{12}$$

B. Chemical Kinetics Mechanisms

The reaction mechanism due to Anderson [22] contains 81 species and 513 reactions and can incur significant computational cost for transient reacting flow computations. Two reductions of this mechanism, RChem1 and RChem2 are considered in the present work. The first mechanism, RChem1 consists of 25 species and 98 reactions while the second reduction RChem2 includes 29 species and 120 reactions [30,31]. MMH oxidation chemistry proceeds through successive hydrogen abstractions to form HONO and daughter species CH_xN_2. The development of these mechanisms is recent and the original as well as the two reduced sets RChem1 and RChem2 consider hydrogen abstraction first from the nitrogen atom attached to the methyl radical, followed by the other nitrogen atom which is then followed by scission of the methyl radical. A third reduced reaction mechanism RChem3 comprising 41 species and 200 reactions is a latest set of reactions for these propellants [46]. Based on the morpholine reaction mechanism due to Li et. al. [26], it allows for different hydrogen abstractions from MMH, including one from methyl radical. Additionally it contains species that are observed to form an aerosol after the initial liquid interactions, thus facilitating simultaneous modeling of the liquid and gas phase chemistry. A broad summary of the three mechanisms is provided in table 1.

Table 1: Reduced chemical mechanisms summary

Mechanism	Species	Reactions
RChem1	25	98
RChem2	29	120
RChem3	41	200

C. Liquid Reaction and Vaporization Model

The reaction of liquid MMH and RFNA is known to yield an aerosol at an elevated temperature of $550\,K$ and higher. The major species measured by Wang and Thynell [7] and by Liu et. al. [24] are CH_3ONO_2, N_2O,H_2O and N_2. Based on these products, a global reaction can be formulated (equation 13) with a heat of combustion of $8\,MJ/kg - MMH$ and an adiabatic flame temperature of $1209\,K$.

$$2\,CH_3NHNH_2 + 4\,HNO_3 \longrightarrow 2\,CH_3ONO_2 + N_2O + 5\,H_2O + 2\,N_2. \tag{13a}$$

Recent observations [47, 48] of gas evolution from a drop of MMH impinging on an RFNA pool indicate a delay of the order of $100\,\mu s$, suggesting that the liquid reaction is complete before then. Due to such short time scales, this interaction has been challenging to probe experimentally. It has been estimated that ionic reactions may precede the decomposition of the intermediates to form the aerosol and hence the activation energy for the global reaction is expected to be negligible. Since the intermediates are known to decompose at a temperature [9] comparable to the boiling point of either liquid, the temperature dependence of the reaction is anticipated to be insignificant, therefore allowing the use of collision frequency, A, as a single parameter for determining the reaction rate. Four values of the collision frequency and corresponding temperature transient are shown in Figure 3(a), indicating that the collision frequency of 10^{16} corresponds to a delay consistent with the observed gas evolution. The rate of the liquid reaction is therefore given as,

$$\begin{aligned} &k_f = AT^b e^{-E_a/RT} \\ &A = 10^{16}; \qquad b = 0.0; \qquad \text{and} \qquad E_a = 0.0 \end{aligned} \tag{14}$$

Vaporization is modeled using the Langmuir expression:

$$\dot{m}_v = \frac{S p_{vref}}{\sqrt{2\pi MWRT}} \mathrm{e}^{\frac{\Delta H_v}{2.303R}\left(\frac{1}{T_{ref}} - \frac{1}{T}\right)} \tag{15}$$

where S is the surface area, p_{vref} is reference vapor pressure at T_{ref}, T is the current liquid temperature, MW is molecular mass, R is universal gas constant and ΔH_v is the heat of vaporization. The surface area of the liquid in the homogeneous equilibrium model relates to the gradient of the volume fraction of the liquid, which in turn varies as the inverse of the cell size, $1/\Delta x$. It is apparent that knowing the properties of fluids, this expression can be easily cast in Arrhenius form, allowing the phase change to be modeled as a chemical transformation where the difference in the enthalpy of the phases provides the expected endothermic behavior. Combining the vaporization model with the liquid reaction for different surface area S (Figure 3(b)) shows that the time scales involved are substantially different and for a premixed liquid, the vaporization is a slow process compared to the liquid reaction.

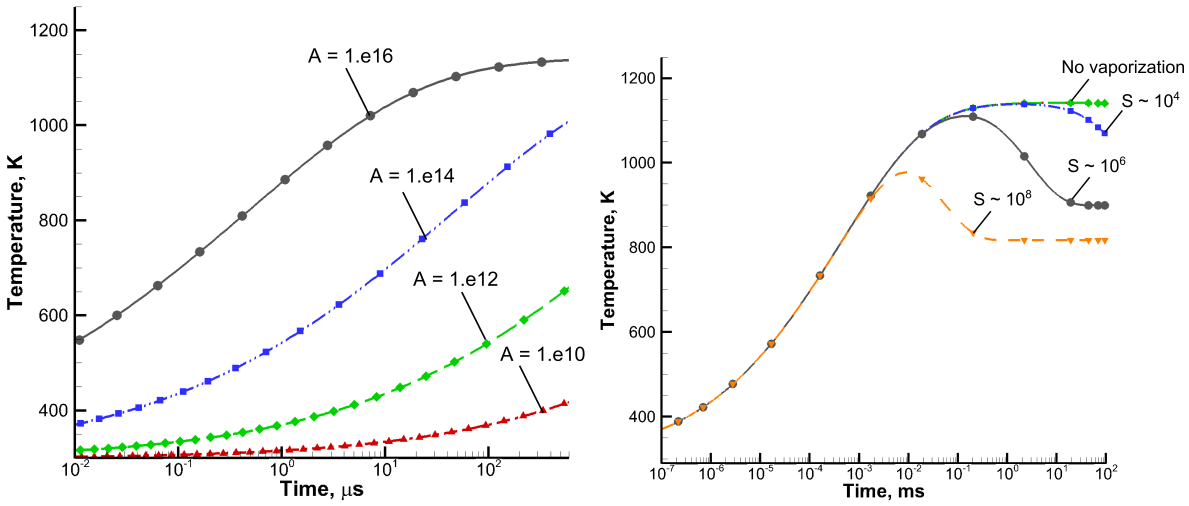

(a) Liquid reaction

(b) Liquid reaction and vaporization

Figure 3: Transient temperature for liquid reaction and vaporization, O/F = 1.5

III. Results and Discussion

In order to develop a systematic framework for a time accurate reacting flow simulation, we begin with autoignition of the premixed reactants. Due to their importance in the vaporizing spray environment, transport phenomena are investigated next using the opposed diffusion flames. Lastly the case of opposed liquid jets of MMH and RFNA is used to explore combined effects of liquid and gas chemistry along with fluid dynamics. This set of cases provides a foundation for subsequent modeling efforts targeting more realistic experimental configurations.

A. Autoignition

The constant volume or constant pressure "bomb" reactor can be modeled as zero dimensional cases in order to explore the transient behavior of premixed propellants. The initial condition is set with a given temperature and composition at a pressure of one atmosphere and the transient solution is sought using the commercial solver Cosilab. In addition to understanding the transient behavior, performance of the reaction mechanisms is also of importance. Particularly relevant for a multi-dimensional time accurate simulation are the initial temperatures, mixture ignition limits and time scales. Validation of a zero dimensional version of the GEMS solver is also carried out by comparing against the transient results from Cosilab.

The main parameters of the reactor problem are the oxidizer to fuel ratio (O/F ratio) and the initial mixture temperature. Wang et. al. [7] found that the aerosol formed due to liquid interactions can reach temperatures of $550\,K$ and ignition in the gas phase is observed beyond this temperature. Figure 4 shows representative results for both constant pressure and constant volume bomb cases. As seen from Figure 4(a), a mixture temperature in excess of $650\,K$ leads to ignition delays consistent with experimental observations and is close to the reported value [49]. Ignition delay predictions by RChem1 and RChem2, shown in Figure 4(a), are close while third mechanism RChem3 predicts a smaller ignition delay at a lower mixture temperatures and has a lesser slope than RChem1 and RChem2. For a stoichiometric mixture, predicted ignition delays match at $700\,K$ for RChem2 and RChem3 and at $730\,K$ for RChem1 and RChem3. In comparison with constant pressure case, transient mixture temperature and pressure for constant volume case are higher for the same heat release and therefore a lower ignition delay is to be anticipated. Comparison of stoichiometric mixtures at various initial temperatures(Figure 4(b)) shows that the constant volume case has a similar trend as the constant pressure case with a factor of two lower ignition delay values.

A typical temperature transient for these propellants is shown in Figure 5(a) for all three reduced mechanisms. It shows evidence of three steps - a pre-ignition first step followed by two steps during ignition. The

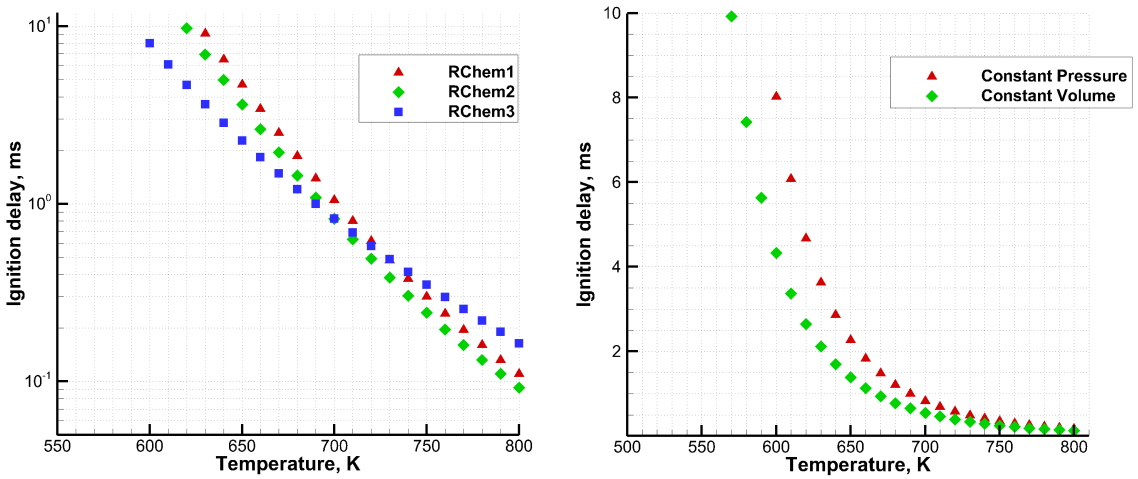

(a) Constant pressure (b) RChem3

Figure 4: Ignition delay predictions for stoichiometric mixture

pre-ignition step starts with a sharp rise followed by a gradual increase to a temperature of 1000 K, while the second step takes the mixture to a temperature of 2500 K, and the last step completes the reactions to near equilibrium condition. As was reported earlier [50], RChem1 predicts a lower temperature than the equilibrium and the third transient is absent for RChem1, delayed for RChem2, while in case of RChem3, the third transient is coincident with the second transient. Initial MMH oxidation occurs through successive hydrogen abstraction by NO_2 while later oxidation occurs through the action of hydroxyl (OH) radical. As seen from Figure 5(b), the OH mass fraction clearly corresponds to the third transient, which is absent for RChem1, delayed for RChem2 and coincident with the second transient for RChem3. This behavior is akin in part to the hydrocarbon chemistry and is a result of the methyl radical in the MMH.

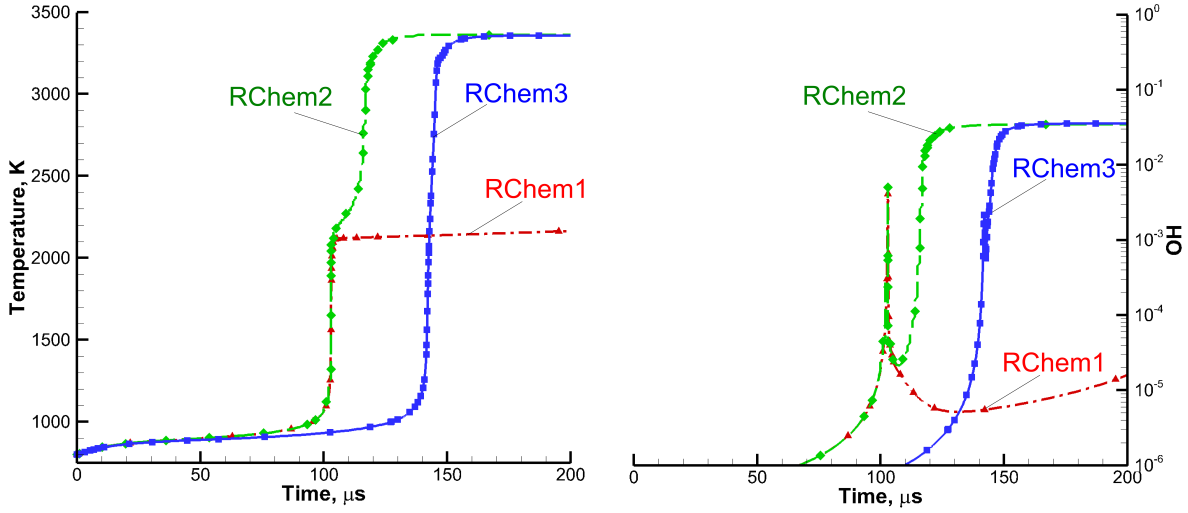

(a) Temperature (b) OH mass fraction

Figure 5: Transient for O/F ratio 1.6

In order to understand the asymptotic state predicted by the three mechanisms, species compositions at two times, 20 μs apart, before and after ignition are plotted against the equilibrium values in Figure 6. Figure 6(a) shows the nitrogen containing species and Figure 6(b) shows the hydroxyl radical and the

products of complete combustion. Comparison of RChem1 and RChem2 shows that, except for NO, the nitrogen containing species predicted by RChem1 move towards equilibrium while RChem2 predicts that the nitrogen containing species are near equilibrium composition even before ignition. Although similar to RChem1, RChem3 differs in that all the nitrogen containing species move closer to equilibrium during the ignition. The hydroxyl radical mole fractions predicted by RChem2 and RChem3 are noted to be closer to the equilibrium values as compared to RChem1 predictions and the resulting product composition is also closer to equilibrium, indicating that the pathways for hydroxyl radical are important.

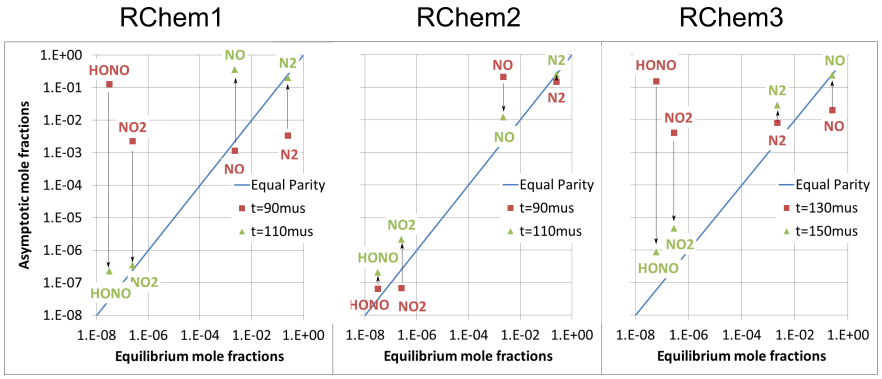

(a)

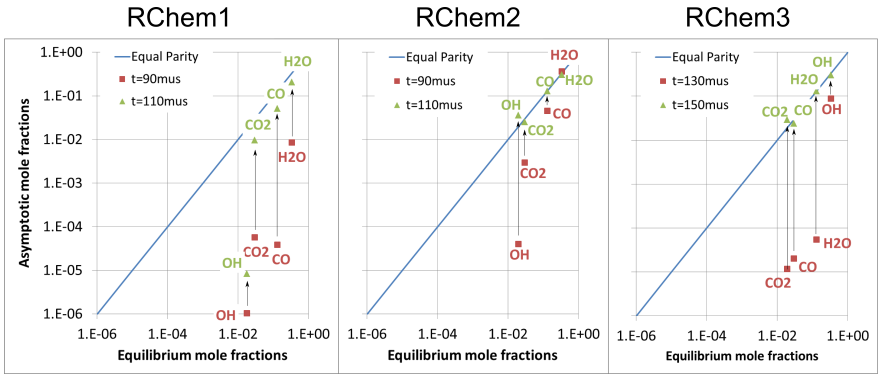

(b)

Figure 6: Species transient for O/F ratio 1.6

Exploring RChem3 in greater depth is necessary for its use with the liquid phase to isolate the effects of liquid reactions and vaporization from the gas phase kinetics. In order to map ignition with RChem3, a range of O/F ratios: 0.1 to 11.0, corresponding to equivalence ratios 25 to 0.25, is considered. The rich end of the O/F ratio represents a fuel droplet vaporizing in an oxidizer rich environment whereas for lean mixtures, a vaporizing oxidizer droplet is enveloped by fuel vapor. Additionally, the initial temperature is known to depend upon the liquid reactions and is varied in this case as a parameter. Corresponding autoignition delay trends are shown in Figure 7. A clear distinction is seen from fuel rich side to oxidizer rich side, confirming historically known behavior that an oxidizer lead has a lower ignition delay Boorady:1967,lecourt2004mmh . It should be noted that the equivalence ratio scale is not linear and comparable limits on the O/F ratio scale are from one to eleven. Within these limits, the fuel rich side exhibits two orders of magnitude difference in the ignition delay for a given initial temperature. The oxidizer rich side shows less than half an order of magnitude difference for the same temperature. The sharpest increase in the ignition delay is three orders of magnitude occurring from stoichiometric condition to an equivalence ratio of $\phi = 3$ at $500\,K$. There is also a difference between initial mixture temperatures below and above $500\,K$. Lower temperatures show an order of magnitude drop in ignition delay per $100\,K$ increase in initial temperature while higher temperatures show less than half an order of magnitude drop for the same increase in initial temperature. This is an important characteristic of these vapors and is expected to influence the ignition in a vaporizing spray.

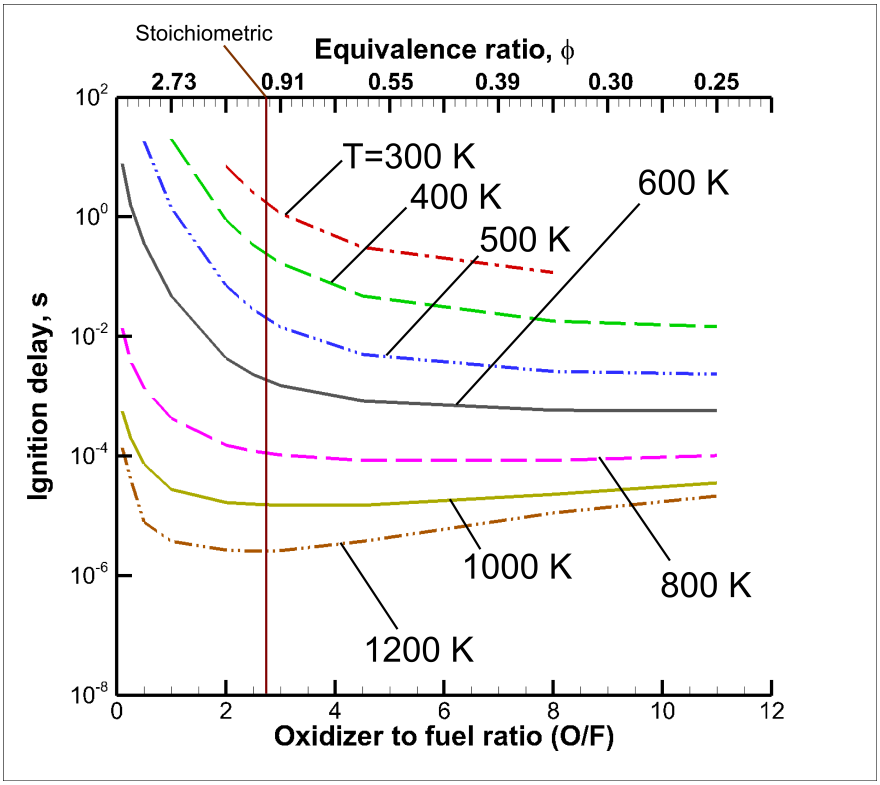

(a)

Figure 7: Variation of ignition delay with O/F ratio and initial mixture temperature

B. Premixed Liquids

Experimental evidence as well as gas phase auto-ignition behavior suggests that liquid reactions provide an initial temperature rise for vaporization of the propellants and act as a trigger for the gas phase chemistry. Therefore a logical next step is to consider premixed liquids at the interface of the two propellants. Temporal evolution of such an interface will be rapid and highly localized, however to isolate and study the underlying transient processes, auto-ignition of the liquid propellants in a homogeneous system can be useful. In this case, premixed liquids with a given composition and at room temperature and pressure are allowed to react and vaporize and the vapors react further to ignite in the gas phase. Liquid phase global reaction is used along with the vaporization model and gas phase kinetics are handled using RChem3, which includes the products of liquid reaction, providing a path to final products of the combustion. Parametric variation of the initial mixture composition is used for mapping the ignition limits while temporal history of the species and temperature illustrate local evolution of the liquid reaction sites.

The transients of some of the intermediate species are shown in Figure 8. Species derived by successive hydrogen abstraction from MMH show an initial decrease at a temperature of 800 K and the radical HNCO is seen to increase from this point till ignition. Catoire [9] found that HNCO can be one of the major species sustaining MMH/RFNA combustion. Indeed, it is seen that the HNCO peak occurs at the peak temperature while HONO, which is known to occur through oxidizer decomposition and successive hydrogen abstraction peaks earlier. Methyl nitrate CH_3ONO_2 decomposition into CH_3O and NO_2, known to be endothermic, is seen before the first drop in the hydroxyl (OH) radical which takes the mixture to approximately 1000 K. Availability of MMH vapor and its successive derivatives depends upon vaporization and these are seen to build up gradually, slowing the ignition from less than 0.2 ms (Figure 7) for premixed vapors at 800 K to 1 ms for the premixed vaporizing liquids.

Figure 9 shows temperature and MMH vapor transients for various initial compositions constituting a parametric evaluation of the O/F ratio. It is seen that the ignition limit on the oxidizer rich side is lowered

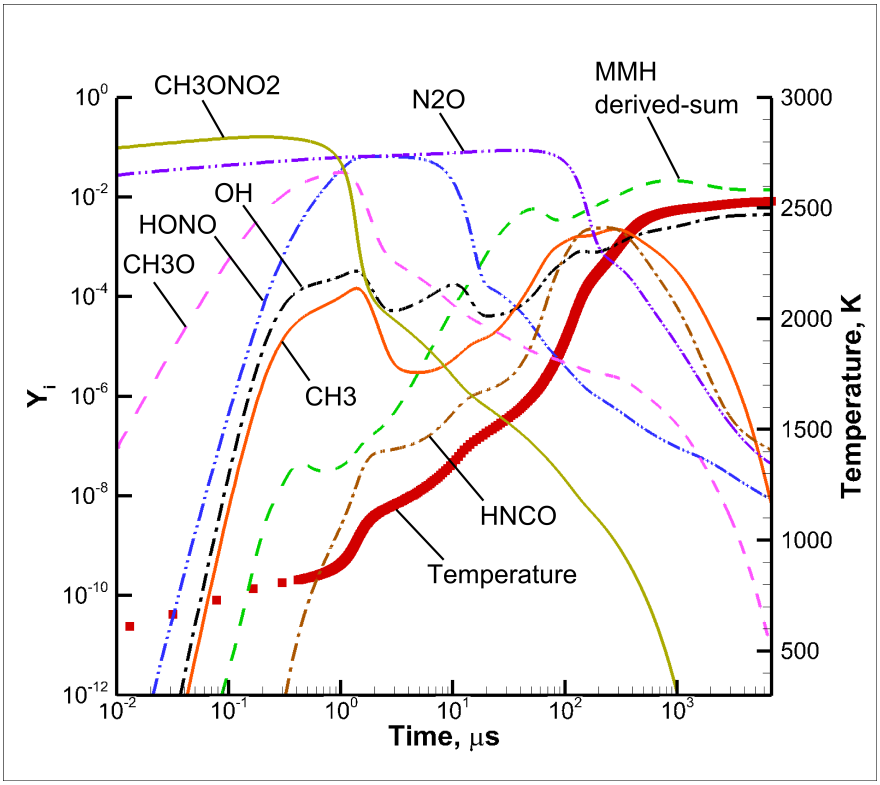

Figure 8: Transient species with liquid reaction and vaporization for O/F = 1.5

from an O/F ratio greater than 11.0 to 9.0. Ignition with vaporizing liquids, unlike premixed gases, is not an instantaneous phenomenon but a cumulative occurrence of pre-ignition reactions. This leads to a continuous temperature increase up to the ignition point in contrast to the almost constant temperature of the pre-ignition gaseous mixtures. At the end of ignitable range (r = 0.15, 3.3) temperature transients lack the sharp initial rise to 1000 K and take two orders of magnitude longer to reach the ignition point where a sharp temperature gradient is observed in contrast to a smooth ignition for near stoichiometric mixtures. Vaporizing sprays can produce this entire range of conditions and can therefore be one of the reasons for sharp pressure increases seen in practice.

C. Opposed Diffusion Flame

Many studies of hypergolicity of this family of propellants [7, 15, 48, 51] have focused on a drop test where a drop of the fuel falls onto a pool of oxidizer or vice versa. A common observation from such tests is the gas evolution at the interface and subsequent gas phase ignition. A vaporizing spray at the extremities of the liquid sheets also produces rich and lean pockets of gaseous mixtures. The length scale of such pockets can be an order of magnitude larger than a vaporizing drop and thus mixing in such regions will be governed by diffusion. Experimental evidence suggests that the diffusion flame of MMH consists of two distinct regions [15, 25] and it has been hypothesized that the first flame-front is due to MMH decomposition and the second flamefront completes oxidation. Therefore, a key step to understanding the physics in the gas layer separating the liquid sheets or the diffusive mixtures elsewhere, is the study of an opposed jet diffusion flame.

A Steady-opposed diffusion flame at different strain rates is considered and a solution over a domain width of 10 cm is obtained with smoothness insured by adaptive gridding based on a gradient parameter of 0.2 and a curvature parameter limited to 0.5. Consistent with previous section, we use a fuel and the oxidizer temperature of 800 K and vary the inlet velocity for the desired strain rate. Structure of the flame is observed using selected species along with the normalized reaction heat rate (HRR) for two of the

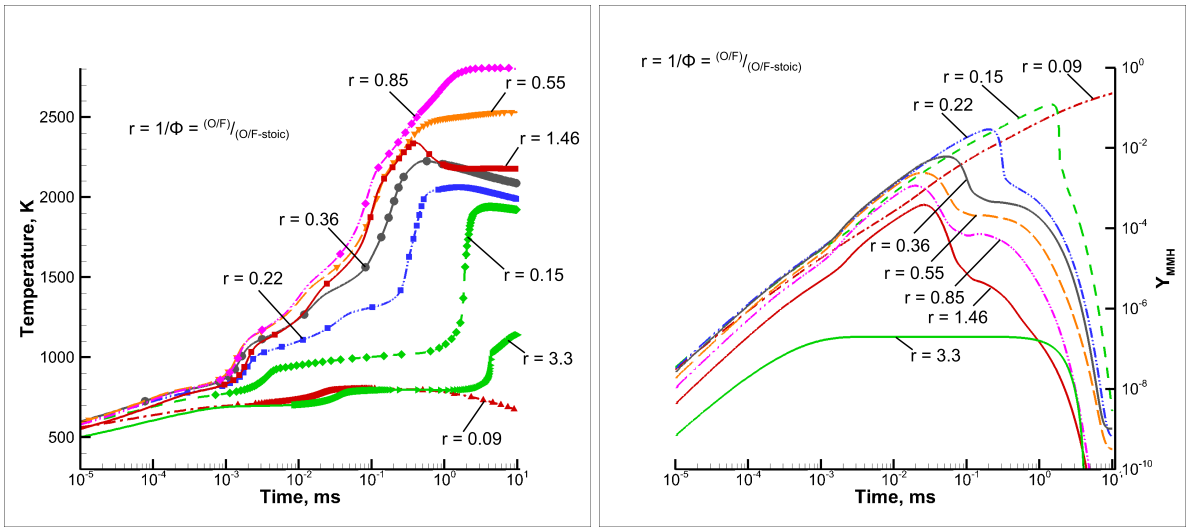

(a) Temperature (b) MMH mass fraction

Figure 9: Transient behavior of premixed reacting and vaporizing liquids as a function of the O/F ratio

mechanisms, RChem1 and RChem3.

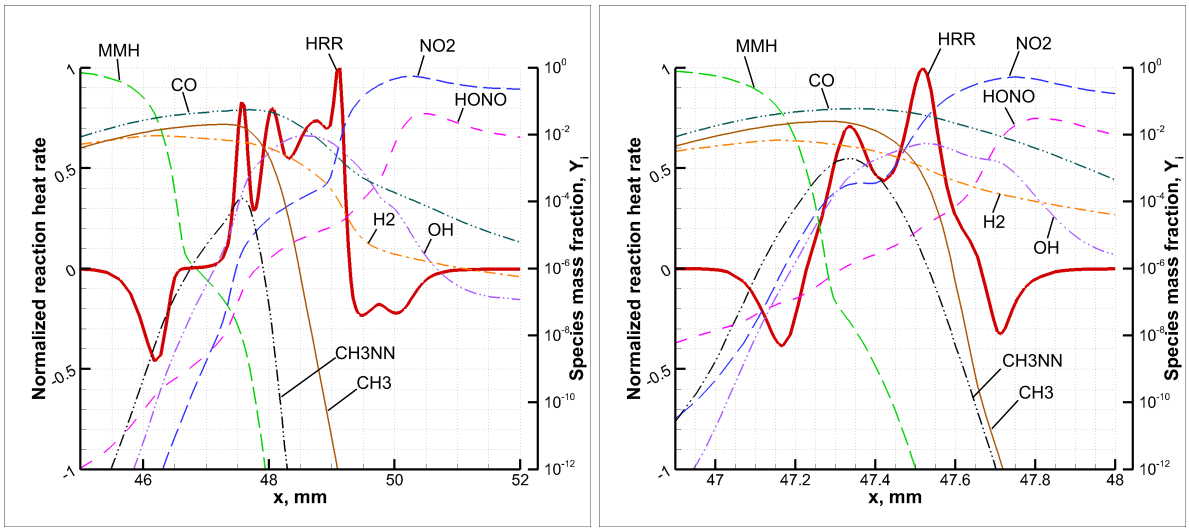

(a) Strain rate = $40\,s^{-1}$ (b) Strain rate = $1280\,s^{-1}$

Figure 10: Normalized heat release rate and species for two strain rates predicted with RChem1

The flame structure predicted with RChem1 for two strain rates is shown in Figure 10. At a low strain rate of $40\,s^{-1}$, the normalized heat release rate (HRR) shows four distinct peaks in the flame region. The first hydrogen abstraction from MMH is known to be endothermic and coincides with the fuel side trough in the HRR and the production of the final MMH derivative species, CH_3NN. After the last non-methyl hydrogen abstraction from MMH, the decomposition proceeds through scission of methyl radical and this step is known to be exothermic. The first peak HRR observed on the fuel side coincides with the destruction of CH_3NN and corresponds to the last step in MMH decomposition. The next HRR peak is coincident with methyl radical destruction which is followed by a CO peak indicative of a two step oxidation process. The last peak HRR corresponds to H_2 and CO oxidation and is the highest. Although HONO formation is

expected to be seen on the fuel side due to hydrogen abstraction, the peak mass fraction of HONO is seen on the oxidizer side due to endothermic dissociation of HNO_3 to OH and NO_2. At a relatively high strain rate of 1280 s^{-1}, the four parts of the flame observed earlier, identified by the peak heat release rate merge to form two, where the first peak in the HRR is coincident with the CH_3NN peak and the second peak corresponds to combined destruction of CH_3NN and CH_3 as well as oxidation of hydrogen and CO. Noting the change in the magnitude of the normalized peaks, it is clear that the major part of the heat release is due to the second HRR peak.

For the same strain rates, predictions with RChem3 are shown in Figure 11. Lower of the two strain rates shows two flame zones identified by peak heat release rates, consistent with the previously observed dual flame of hydrazine and N_2O_4 [15] and MMH RFNA combustion seen during experimental studies at Purdue university. The fuel side peak heat release rate is the highest and clearly corresponds to MMH decomposition. Unlike RChem1, MMH decomposition through successive H abstraction takes place within this region and CH_3 mass fraction remains nearly constant up to a diminished second peak where it gets destroyed with CO mass fraction reaching a peak value. The second highest heat release rate corresponds to oxidation of CO and H_2 by OH and NO_2. In this case, the HONO concentration drops significantly in the second peak, indicating that alternative pathways in RChem3 for MMH decomposition are effective. Also noticeable are the two endothermic regions on the oxidizer side, which are comparable in magnitude to the peak HRR and can potentially alter ignition behavior in case of a multi-dimensional simulation. At a higher strain rate, the flame zone consists of a single prominent peak corresponding to oxidation of H_2 and CO in addition to diminished HRR peaks corresponding to MMH decomposition, CH_3 destruction and conversion of remaining derivatives of MMH. A notable difference between the predictions of RChem1 and RChem3 for both strain rates is the absence of an endothermic region adjoining the flame on the fuel side. For both strain rates, the width of the flame predicted by RChem3 is twice that of RChem1, suggesting a need of uniform higher spatial resolution in multi-dimensional simulations.

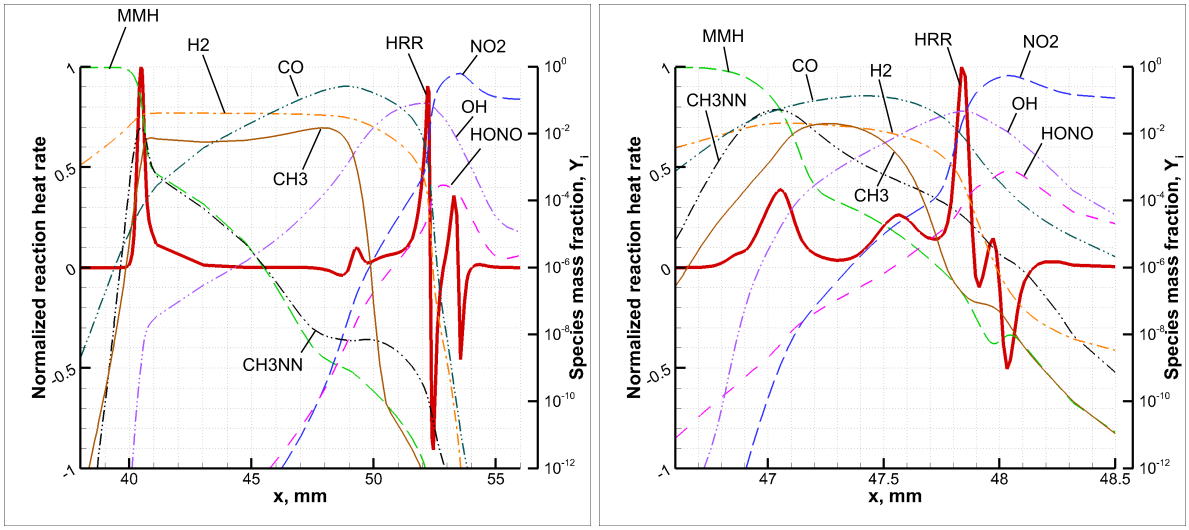

(a) Strain rate = 40 $s^{-}1$

(b) Strain rate = 1280 $s^{-}1$

Figure 11: Normalized heat release rate and species for two strain rates predicted with RChem3

D. Opposed Liquid Jets

Liquid sprays and injectors have been previously studied [52–57] but there has been limited inclusion of liquid-phase reactions in modeling efforts targeting hypergolic ignition. As found from experimental evidence and theoretical computations, liquid interaction is a key process in hypergolic ignition of these propellants. For an impinging jet injector, there are two regions of such interaction, the first being the impingement point and unstable sheets formed thereafter while the second is the less intuitive spray interaction at the extremities of the liquid sheets where photographic evidence [10] suggests that droplet collisions lead to

multitudes of micro-explosion events [28, 58], triggering gas phase ignition. While the later interactions are substantially challenging to investigate, prior interaction can be numerically studied for liquid contact, extent of liquid reaction, resulting gas layer and its temperature. It is well known that liquid diffusion is an order of magnitude slower than gas diffusion, making the liquid reactions a surface phenomenon. Mixing through convective transport is therefore the primary avenue of liquid interaction which in turn depends upon gas layer formation and interface dynamics. Interdependence of heat generation and gas layer formation needs to be investigated to determine conditions in the gas layer separating the liquid sheets that are formed upon impingement.

The impinging jet injector is one of the favored types of injectors for these propellants and building towards that, two-dimensional opposed impinging liquid sheets are considered first. The sheet width is assumed to be $0.25\,mm$ which is a third of the orifice radius of the injector. The span separating the impinging jets is $1\,mm$ and open to atmospheric condition. Relatively smaller dimensions are specified in this case for managing the computational expense of obtaining a grid independent solution. The behavior of reacting vaporizing liquids is considered without the additional expense of gas phase chemistry. Plug flow of liquids at $300\,K$ is specified at the boundaries so as to have equal momentum of the impinging streams. Resulting velocities are $15\,m/s$ for RFNA and $20\,m/s$ for MMH due to the density difference between the two fluids. To isolate the effect of the gas-liquid interface, turbulence is not considered. For grid independent solution of the gas layer between the liquids, a series of grids is chosen. It is found that a grid of cell size $1\,\mu m$ provides sufficient resolution and there are 5 to 8 cells within the gas layer. With this grid, the computation is carried out and transient and average quantities are monitored.

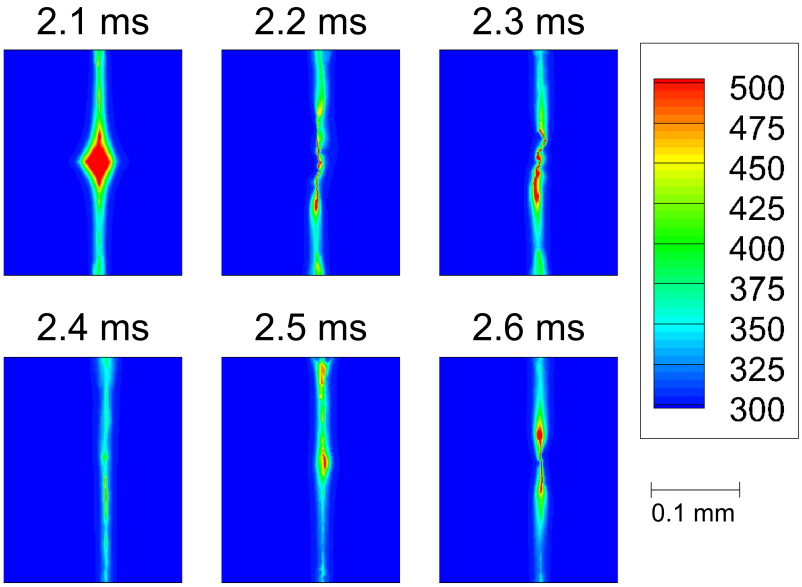

Figure 12: Resolved transient liquid-gas interface

A series of transient temperature contours (Figure 12) shows that after initial planar contact, the interface rapidly becomes corrugated, resulting in rolling up of liquids at multiple sites. Such sites react violently to produce gas bubbles which are squeezed out by the incoming liquid. Although initial contact and mixing leads to temperatures in excess of $500\,K$, rapid bubble generation prevents further contact of the two liquids and the gas layer cools down to a temperature of less than $450\,K$ as seen from averaged results (Figure 13) for two grid-sizes.

Parametric experimental investigation [59] of jet diameter and velocity have shown that adequate liquid contact is critical for repeatable ignition and modeling can help understanding hypergolic ignition further, which is necessary to design injectors that are capable of rapidly repeatable cyclic ignition. It should be kept in mind that there are two clear distinctions in the case of the impinging jet setup - firstly, three dimensionality which allows for additional expansion and slowdown of the sheets and secondly, a component of momentum along the jet axis which causes shear layer development and enhances mixing. In the region

close to the impingement point however, as the gas layer acts to support transverse momentum of the jets, it is likely that rapid contact and limited heat generation, as seen from this case will prevail. Future studies will focus on extending these results to three dimensional impinging jet configurations. Preliminary results for gas-phase propellants are presented in a companion article in this conference. Liquid-phase computations will be undertaken in the near future and will be closely tailored to current experimental studies at Purdue university.

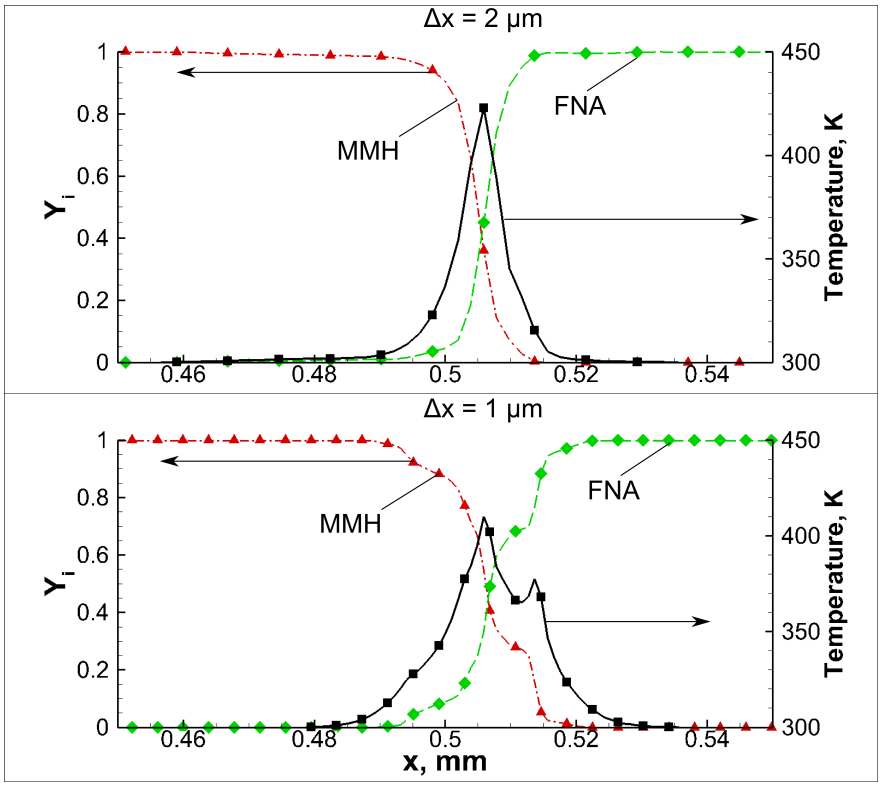

Figure 13: Average temperature and reactant mass fractions at the liquid-gas interface

IV. Summary

Three fundamental problems - autoignition, opposed diffusion flame and liquid opposed jets, are investigated for understanding the ignition phenomenon of hypergolic propellants MMH and RFNA. Gas phase auto-ignition is modeled with three reduced kinetics mechanisms and shows an initial temperature requirement of $650\,K$. With respect to mixture composition, the ignition delay is observed to increase sharply for fuel rich mixtures while fuel lean mixtures show the ignition delay to be relatively independent of initial composition. This is in agreement with the established practice of providing an oxidizer rich environment for ignition of MMH-RFNA combinations. Gas phase ignition by virtue of its initial temperature requirement, depends upon liquid reaction for activation and including a liquid reaction and vaporization shows different behavior than the premixed gas auto-ignition. Unlike the premixed, pre-heated gaseous reactants, which showed pre-ignition reactions at an almost constant temperature, the homogeneous liquid mixture shows continuous pre-ignition temperature rise, recovering the step like temperature transient in the limit of rich and lean mixture extremes. In case of a practical device, operating outside the continuous temperature increase regime may be an issue for achieving repeatable smooth ignition.

The opposed diffusion flame investigation indicates multiple zones of heat release corresponding to various aspects of the chemistry. At low strain the zones corresponding to MMH decomposition and subsequent methyl, CO and hydrogen oxidation are distinct and have comparable heat release. High strain rate on the other hand shows merging of several regions, particularly on the oxidizer side, with a diminished contribution

from MMH decomposition. An endothermic region exists adjacent to the oxidizer side and can act as a delaying mechanism for the ignition of the diffusing reactants.

Opposed liquid jets provide a further insight into liquid mixing, reaction and dynamics of the gas layer trapped between liquid sheets. The gas layer develops as initial products formed from liquid reaction cannot stably support the momentum of the liquid jets, leading to intermittent contact and bubble formation between the two liquids. Local temperatures can exceed the lower threshold of the gas phase ignition but average temperatures in two dimensional sheets are seen to be restricted to $450\,K$. Future work will focus on extending these results to practical three dimensional experimental configurations, wherein additional effects may contribute to the occurrence of ignition.

Acknowledgments

The author is grateful for the support provided for this work by the United States Army Research Office under the Multidisciplinary University Research Initiative grant number W911NF-08-1-0171 with Dr. Ralph Anthenien as program manager. The author also wishes to acknowledge Prof. Westmoreland and Nicole Labbe for helpful discussions and for providing the reduced chemical mechanisms.

References

[1]Raymond L. Chuan and Paul C. Wilber. Ignition of hypergolic propellants in a simulated space environment. *Journal of Spacecraft*, 7(2):282 – 284, 1966.

[2]Warren Juran and R. Carl Stechman. Ignition transients in small hypergolic rockets. *Journal of spacecraft*, 5(3):288 – 292, 1967.

[3]F. A. Boorady and D. A. Douglass. Solution of the high-vacuum hard -start problem of the irfna-udmh rocket for gemini agena. *Journal of spacecraft*, 5(1):22 – 30, February 1967.

[4]T.R. Mills, B. P. Breen, E. A. Tkachenko, and B. R. Lawver. Transients influencing rocket engine ignition and popping. Technical report, NASA, 1969.

[5]R. Lecourt and F.X. d'Herbigny. MMH/NTO injection and ignition in vacuum downstream from an aestus engine single injection element. *Aerospace science and technology*, 8(3):207–217, 2004.

[6]M.A. Saad, G.J. Antonides, and S.R. Goldwasser. Effect of pressure on ignition of hypergolic liquid propellants. Technical report, DTIC Document, 1973.

[7]SQ Wang and ST Thynell. An experimental study on the hypergolic interaction between monomethylhydrazine and nitric acid. *Combustion and Flame*, 2011.

[8]Smith J.E. Time resolved measurements and reactive pathways of hypergolic bipropellant combustion. Technical report, DTIC Document, 2006.

[9]Laurent Catoire, Steven D Chambreau, and Ghanshyam L Vaghjiani. Chemical kinetics interpretation of hypergolicity of dicyanamide ionic liquid-based systems. *Combustion and flame*, 159(4):1759–1768, 2012.

[10]Heister S.D. abd Pourpoint T.L. Progress in understanding the combustion physics for gelled hypergolic propellants. In *5th European Conference on Aerospace Sciences (EUCASS), Munich, Germany*, 2013.

[11]G. B. Skinner, W. H. Hedley, and A. D. Snyder. Mechanism and chemical inhibition of the hydrazine-nitrogen tetroxide reaction. Technical report, Armed Services Technical Information Agency, 1962.

[12]Marshall C. Burrows. Mixing and reaction studies of hydrazine and nitrogen tetroxide using photographic and spectral techniques. Technical note, NASA, 1967.

[13]Wataru Daimon and Itsuro Kimura. A study of pressure waves and explosions induced by contact of hypergolic liquid propellants. *Symposium (International) on Combustion*, 19(1):749 – 756, 1982.

[14]L. B. Zung, E. A. Tkachenko, and B. P. Breen. A basic study on the ignition of hypergolic liquid propellants. Technical report, National Aeronautics and Space Administration, 1968.

[15]B.R. Lawver. Some observations on the combustion of N_2H_4 droplets(combustion of hydrazine droplets burning in hydrazine vapor investigated via suspended droplet technique). *AIAA JOURNAL*, 4:659–662, 1966.

[16]MB Detweiler and MA Saad. Analysis of N_2H_4-rfna reaction product. *AIAA Journal*, 7:1588–1592, 1969.

[17]R.F. Sawyer and I. Glassman. Gas-phase reactions of hydrazine with nitrogen dioxide, nitric oxide, and oxygen. In *Symposium (International) on Combustion*, volume 11, pages 861–869. Elsevier, 1967.

[18]S. Zabarnick. Kinetics of the reaction $OH + NO + M \longrightarrow HONO + M$ as a function of temperature and pressure in the presence of argon, sf6, and n2 bath gas. *Chemical physics*, 171(1-2):265–273, 1993.

[19]L. Catoire, X. Bassin, G. Dupre, and C. Paillard. Experimental study and kinetic modeling of the thermal decomposition of gaseous monomethylhydrazine. application to detonation sensitivity. *Shock Waves*, 6(3):139–146, 1996.

[20]R.D. Cook, S.H. Pyun, J. Cho, D.F. Davidson, and R.K. Hanson. Shock tube measurements of species time-histories in monomethyl hydrazine pyrolysis. *Combustion and Flame*, 2011.

[21]L. Catoire, T. Ludwig, X. Bassin, G. Dupre, and C. Paillard. Kinetic modeling of the ignition delays in monomethylhydrazine/oxygen/argon mixtures. In *Symposium (International) on Combustion*, volume 27, pages 2359–2365. Elsevier, 1998.

[22]W.R. Anderson, M.J. McQuaid, M.J. Nusca, and A.J. Kotlar. A detailed, finite-rate, chemical kinetics mechanism for monomethylhydrazine-red fuming nitric acid systems. Technical report, DTIC Document, 2010.

[23]Antoine Osmont, Laurent Catoire, Thomas M Klapötke, Ghanshyam L Vaghjiani, and Mark T Swihart. Thermochemistry of species potentially formed during nto/mmh hypergolic ignition. *Propellants, Explosives, Pyrotechnics*, 33(3):209–212, 2008.

[24]Wei-Guang Liu, Shiqing Wang, Siddharth Dasgupta, Stefan T Thynell, William A Goddard III, Sergey Zybin, and Richard A Yetter. Experimental and quantum mechanics investigations of early reactions of monomethylhydrazine with mixtures of NO_2 and N_2O_4. *Combustion and Flame*, 2013.

[25]Daimon Yu, Terashima Hiroshi, and koshi mtsuo. Chemical kinetics of hypergolic ignition in hydrazine/nitrogen-dioxide gas mixtures. In *51st AIAA Aerospace Sciences Meeting including the New Horizons Forum and Aerospace Exposition*.

[26]Sijie Li, David F Davidson, Ronald K Hanson, Nicole J Labbe, Phillip R Westmoreland, Patrick Oßwald, and Katharina Kohse-Höinghaus. Shock tube measurements and model development for morpholine pyrolysis and oxidation at high pressures. *Combustion and Flame*, 2013.

[27]Labbe N. *Determining detailed reaction kinetics for nitrogen- and oxygen-containing fuels*. PhD thesis, UMass Amberst, 2013.

[28]Dambach E. M. *Ignition of Hypergolic Propellants*. Ph.D. Thesis, Purdue University, W. Lafayette, IN, 2010.

[29]Angelo J Alfano, Jeffrey D Mills, and Ghanshyam L Vaghjiani. Highly accurate ignition delay apparatus for hypergolic fuel research. *Review of scientific instruments*, 77(4):045109–045109, 2006.

[30]Y. Kim N. Labbe and P. Westmoreland. Computational mechanism development for hypergolic propellant systems: Mmh and dmaz, 2010.

[31]P. Westmoreland and N. Labbe. Task 3.2 reaction kinetics studies. private communication, 2010.

[32]S. Venkateswaran, J.W. Lindau, R.F. Kunz, and C.L. Merkle. Computation of multiphase mixture flows with compressibility effects. *Journal of Computational Physics*, 180(1):54–77, 2002.

[33]Y.H. Choi and C.L. Merkle. The application of preconditioning in viscous flows. *Journal of Computational Physics*, 105(2):207–223, 1993.

[34]D. Li, V. Sankaran, J.W. Lindau, and C.L. Merkle. A unified computational formulation for multi-component and multi-phase flows. In *43 rd AIAA Aerospace Sciences Meeting and Exhibit*, 2005.

[35]Lian C., Xia G., and Merkle C.L. Impact of source terms on reliability of cfd algorithms. *Computers and Fluids*, 39(10):1909–1922, 2010.

[36]Matthew E. Harvazinski. *Modeling self-excited combustion instabilities using a combination of two- and three-dimensional simulations*. PhD thesis, Purdue University, 2012.

[37]S.R. Turns. *An introduction to combustion: concepts and applications*, volume 10. McGraw-hill New York, 1996.

[38]J. Troe. Predictive possibilities of unimolecular rate theory. *Journal of Physical Chemistry*, 83(1):114–126, 1979.

[39]RG Gilbert, K. Luther, and J. Troe. Theory of thermal unimolecular reactions in the fall-off range. ii. weak collision rate constants. *Berichte der Bunsengesellschaft für physikalische Chemie*, 87(2):169–177, 1983.

[40]W. Tsang and J.T. Herron. Chemical kinetic data base for propellant combustion. i. reactions involving NO, NO_2, HNO, HNO_2, HCN and N_2O. *J. Phys. Chem. Ref. Data*, 20(4):609–663, 1991.

[41]B.J. McBride, M.J. Zehe, and S. Gordon. *NASA Glenn coefficients for calculating thermodynamic properties of individual species*. National Aeronautics and Space Administration, John H. Glenn Research Center at Lewis Field, 2002.

[42]S. Chapman and T.G. Cowling. *The mathematical theory of non-uniform gases: an account of the kinetic theory of viscosity, thermal conduction, and diffusion in gases*. Cambridge Univ Pr, 1991.

[43]J.O. Hirschfelder, R.B. Bird, and E.L. Spotz. The transport properties of gases and gaseous mixtures. ii. *Chemical Reviews*, 44(1):205–231, 1949.

[44]R.B. Bird, W.E. Stewart, and E.N. Lightfoot. Transport phenomena. 1960. *Madison, USA*, 1960.

[45]S. Mathur, PK Tondon, and SC Saxena. Thermal conductivity of binary, ternary and quaternary mixtures of rare gases. *Molecular physics*, 12(6):569–579, 1967.

[46]P. Westmoreland and N. Labbe. Task 3.2 reaction kinetics studies. private communication, 2012.

[47]Forness J., Pourpoint T.L., and S.D. Heister. Experimental study of impingement and reaction of hypergolic droplets. In *49th AIAA/ASME/SAE/ASEE Joint Propulsion Conference Exhibit*. American Institute of Aeronautics and Astronautics, 2013.

[48]Forness J. Phenomena resulting from hypergolic contact. Master's thesis, Purdue University, August 2013.

[49]Dennis J., Pourpoint T., and Son S. Ignition of gelled monomethylhydrazine and red fuming nitric acid in an impinging jet apparatus. In *47th AIAA/ASME/SAE/ASEE Joint Propulsion Conference and Exhibit*, 2011.

[50]S.V. Sardeshmukh, S.D. Heister, G. Xia, and C. Merkle. Kinetic modeling of hypergolic propellants using impinging element injectors. In *48th AIAA/ASME/SAE/ASEE Joint Propulsion Conference Exhibit*. American Institute of Aeronautics and Astronautics, 2012.

[51]Wataru Daimon, Yoshifumi Gotoh, and Itsuro Kimura. Mechanism of explosion induced by contact of hypergolic liquids. *Journal of Propulsion and Power*, 7(6):946 – 952, 1991.

[52]L.M. Larosiliere and S.M. Jeng. Combustion and flow modelling applied to the OMV VTE. In *Center for Advanced Space Propulsion Second Annual Technical Symposium Proceedings*, pages 15 – 22. NASA, 1990.

[53]J. Steelant and R. Schmehl. Computational modelling of the preflow phase during start-up of an upper-stage rocket engine. In *Fifth European Symposium on Aerothermodynamics for Space Vehicles*, volume 563, page 471, 2005.

[54]V. Yang. *Liquid rocket thrust chambers: aspects of modeling, analysis, and design*, volume 200. Aiaa, 2004.

[55]A.J. Przekwas. Theoretical modeling of liquid jet and sheet breakup processes. *Recent advances in spray combustion: Spray atomization and drop burning phenomena.*, 1:211–239, 1996.

[56]SK Aggarwal. A review of spray ignition phenomena: present status and future research. *Progress in Energy and Combustion Science*, 24(6):565–600, 1998.

[57]G.A. Dressler and J.M. Bauer. Trw pintle engine heritage and performance characteristics. *AIAA Paper*, 3871:2000, 2000.

[58]Erik M Dambach, Yair Solomon, Stephen D Heister, and Timothée L Pourpoint. Investigation into the hypergolic ignition process initiated by low weber number collisions. *Journal of Propulsion and Power*, pages 1–8, 2013.

[59]T. D. Kubal. *Characterization of rheological and ignition properties of hypergolic propellants*. Ph.d. Thesis, Purdue University, W. Lafayette, IN, 2010. Kubal, Travis Daniel; 9781124516240; Copyright ProQuest, UMI Dissertations Publishing 2010; 1489556; 2301056131; 2010; 66569; 858361994; 54059611; English; M1: M.S.M.E.; M3: 1489556.